J. Fluid Mech. (1973), *vol.* 58, *part* 3, *pp.* 595–621
Printed in Great Britain

Axisymmetric waves in compressible Newtonian liquids contained in rigid tubes: steady-periodic mode shapes and dispersion by the method of eigenvalleys

By H. A. SCARTON
Mechanics Division, Rensselaer Polytechnic Institute, Troy, N.Y.
AND W. T. ROULEAU
Department of Mechanical Engineering, Carnegie-Mellon University

(Received 9 July 1971 and in revised form 2 March 1972)

In this paper the first thirty-two axisymmetric modes for steady-periodic waves in viscous compressible liquids contained in rigid, impermeable, circular tubes are calculated. These results end long speculation over the effects of viscosity on guided acoustic waves. Sixteen of the modes belong to a family of rotation-dominated modes whose existence was previously unknown. The thirty-two modes were computed for a wide range of frequencies, viscosities and wavelengths.

The modes were found through the use of the method of eigenvalleys, which also led to the discovery of backward-propagating waves, an exact analytical expression for the zeroth rotational mode eigenvalue, definitive boundaries between low and intermediate frequencies and between intermediate and high frequencies, and a new type of boundary layer, called a dilatational boundary layer.

1. Introduction

In recent years much attention has been focused on the propagation of small amplitude steady-periodic pressure waves through fluids confined in rigid tubes. Although a problem long of intrinsic interest to acousticians, most of the recent research has been spurred on by technological developments in fluid transmission lines and acoustic delay lines, and the desire for better mathematical models of biological flows, particularly arterial blood flow. The effects of viscosity cannot be ignored in these applications, in contrast to the customary acoustic approach. But in the few instances where viscosity has been considered, the analyses have been confined to simplified dynamic models (e.g. quasi-steady and/or plane pressure waves have been assumed), or else incomplete. This paper contains a complete study of the viscous effects for a compressible liquid.

Limited solutions to simplified versions of the problem have been obtained by Kirchhoff (1868), Rayleigh (1896, § 350), Iberall (1950), Shields, Lee & Wiley (1965), Tijdeman (1969) and Rubinow & Keller (1971). Many of the restrictive assumptions were removed by Elco & Hughes (1962) and Cohen & Tu (1962),

who obtained the proper dispersion relation, although they could not solve it except for certain limiting cases. The closest attempt at solution was by Gerlach & Parker (1967), who showed the existence of some of the higher linear symmetric modes of propagation. Unfortunately, owing to inaccuracies in both their computer program and their method, Gerlach & Parker's dispersion curves are in error by several orders of magnitude except for very low frequencies.

Correct eigenvalues and dispersion curves are obtained in this paper for the first thirty-two modes. Backward-propagating waves are found to exist. In addition to the expected eigenvalues, a heretofore unknown second family or 'band' of eigenvalues is also found, and the physical implications are discussed. The method of eigenvalleys is employed to extract these eigenvalues.

2. Analysis

Consider a compressible Newtonian liquid undergoing very small amplitude† steady-periodic laminar‡ oscillation. For a density perturbation ρ much smaller than the constant steady-state density ρ_0, and for a fluid perturbation velocity $\mathbf{v}$ whose modulus is much smaller than the speed of sound $c_0 = (\beta/\rho_0)^{\frac{1}{2}}$, where β is the isothermal bulk modulus, the continuity, state and momentum equations reduce to the linear acoustic equations

$$\frac{\partial \rho}{\partial t} + \rho_0 \nabla . \mathbf{v} = 0, \quad \frac{dp}{d\rho} = \frac{\beta}{\rho_0}, \quad \frac{\partial \mathbf{v}}{\partial t} = -\frac{1}{\rho_0}\nabla p - \nu \nabla \times \nabla \times \mathbf{v} + (\nu' + \tfrac{4}{3}\nu)\nabla(\nabla . \mathbf{v}), \tag{1a,b,c}$$

where the first and second coefficients of kinematic viscosity ν and ν' are assumed constant. The velocity field can be represented as

$$\mathbf{v} = \nabla\phi + \nabla \times \boldsymbol{\psi}. \tag{2}$$

Equations for the scalar potential ϕ and vector potential $\boldsymbol{\psi}$ have been derived by Cohen & Tu (1962), Elco & Hughes (1962), Gerlach & Parker (1967) and Scarton (1970). Substituting (2) into the divergence of (1*c*) leads to the scalar potential wave equation

$$\left[\left(1 + \frac{1}{\omega_0}\frac{\partial}{\partial t}\right)\nabla^2 - \frac{1}{c_0^2}\frac{\partial^2}{\partial t^2}\right]\phi = 0, \quad \omega_0 = \frac{c_0^2}{\nu' + \frac{4}{3}\nu}, \tag{3a,b}$$

in which $\boldsymbol{\psi}$ does not appear. Except for the added viscous term $\omega_0^{-1}\partial(\nabla^2\phi)/\partial t$, equation (3) is identical to the well-known inviscid compressible scalar potential wave equation.

With no circumferential velocity and with axisymmetry, the vector potential will be assumed to possess only the angular component ψ_θ. Taking the curl of (1*c*)

† Acoustic streaming will not occur if the maximum fluid displacements are less than all modal wavelengths.

‡ H. Daneshyar of the University of Cambridge Engineering Laboratories (1971, private communication) has found experimentally that such a flow will not be turbulent if $\{(\nu/RV)\,[1250 + 343R(\omega/\nu)^{\frac{1}{2}}]\}^{-1} < 1$ in the range $0 \leqslant R(\omega/\nu)^{\frac{1}{2}} \leqslant 37$, V being the amplitude of the radially averaged velocity, ν the kinematic viscosity, R the tube radius and ω the radian frequency. This work confirms to within experimental accuracy the work by Sergeev (1966), which shows that laminar conditions exist if $[(\nu/RV)\,(1250 + 1{\cdot}73R^2\omega/\nu)]^{-1} < 1$ for $R(\omega/\nu)^{\frac{1}{2}} < 4$, and $[353(\nu/V)\,(\omega/\nu)^{\frac{1}{2}}]^{-1} < 1$ for $40 > R(\omega/\nu)^{\frac{1}{2}} > 8$.

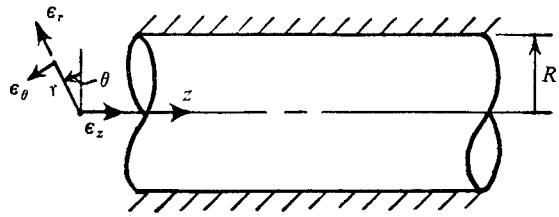

FIGURE 1. Rigid impermeable tube containing a viscous compressible liquid.

and combining this with (2) and the gauge condition $\nabla.\boldsymbol{\psi} = 0$ leads to the diffusion equation for the non-trivial angular component of the vector potential

$$\left[\nabla^2 - \frac{1}{r^2} - \frac{1}{\nu}\frac{\partial}{\partial t}\right]\psi_\theta = 0, \tag{4}$$

in which ϕ does not appear. Hence, (3) and (4) are completely uncoupled.

If the problem is restricted to propagation in a rigid non-porous right-circular cylindrical waveguide (figure 1), the general radial boundary conditions are (i) boundedness at zero radius; (ii) non-porous rigid wall, $v_r(R) = 0$; (iii) no slip at the wall, $v_z(R) = 0$. These viscous boundary conditions at the wall will couple the solutions of (3) and (4) through (2).

If the fluid column is excited by an axisymmetric surface undergoing cyclic oscillation, the solution for the fundamental frequency, along with the solution for each of the higher overtones, can be represented by a steady-periodic separable solution, provided that no temporal instabilities are present and all transient effects have diminished so that the motion has become well established. For the given linear system of differential equations, the form of the separable solution for a typical field quantity $f(r, z, t)$ reduces to

$$f(r, z, t) = \mathrm{Re}\,(f(r)\, e^{i\omega t + kz}), \tag{5}$$

where ω is the *radian frequency* of the fundamental or one of the overtones of the oscillating source, $k = k_r + ik_i$ is the complex *propagation constant* (alternatively called the *eigenvalue*, *separation constant* or *wavenumber*).

Application of (5) to (3) yields the bounded (at $r = 0$) solution for the scalar potential

$$\phi(r, z, t) = \mathrm{Re}\,(C_1 J_0(mr)\, e^{i\omega t + kz}), \tag{6}$$

where the radial solution $J_0(mr)$ is the ordinary zeroth-order Bessel function of the first kind, the complex constant m is the principal square root of

$$m = \left[k^2 + \frac{\omega^2}{c_0^2}\frac{1}{1 + i\omega/\omega_0}\right]^{\frac{1}{2}}, \tag{7}$$

and C_1 is a complex constant of integration.

Application of (5) to (4) yields the bounded (at $r = 0$) solution for the θ component of the vector potential as

$$\psi_\theta(r, z, t) = \mathrm{Re}\,(C_2 J_1(\alpha r)\, e^{i\omega t + kz}), \tag{8}$$

where the radial solution $J_1(\alpha r)$ is the ordinary first-order Bessel function of the first kind, the complex constant α is the principal square root of

$$\alpha = [k^2 - i\omega/\nu]^{\frac{1}{2}}, \tag{9}$$

and C_2 is a complex constant of integration.

Relations for the radial and axial velocity, perturbation pressure, perturbation density and vorticity $\boldsymbol{\Omega} = \nabla \times \mathbf{v}$† are easily obtained from (6) and (8). These are

$$v_r(r,z,t) = -\mathrm{Re}\left[(C_1 m J_1(mr) + C_2 k J_1(\alpha r))\, e^{i\omega t + kz}\right], \tag{10}$$

$$v_z(r,z,t) = \mathrm{Re}\left[(C_1 k J_0(mr) + C_2 \alpha J_0(\alpha r))\, e^{i\omega t + kz}\right], \tag{11}$$

$$p(r,z,t) = \mathrm{Re}\,(C_3 J_0(mr)\, e^{i\omega t + kz}), \quad C_3 = -C_1 i\rho_0 \omega/(1 + i\omega/\omega_0), \tag{12a,b}$$

$$\rho(r,z,t) = c_0^{-2} p(r,z,t), \tag{13}$$

$$\Omega_\theta(r,z,t) = \mathrm{Re}\,(C_4 J_1(\alpha r)\, e^{i\omega t + kz}), \quad \Omega_z = \Omega_r = 0, \quad C_4 = -i(\omega/\nu)\, C_2. \tag{14a,b,c}$$

To ascertain the value of the complex propagation constant k, the two homogeneous zero-speed boundary conditions at the wall are applied to give

$$\begin{bmatrix} v_r(R,z,t) \\ v_z(R,z,t) \end{bmatrix} = \begin{bmatrix} 0 \\ 0 \end{bmatrix} = \mathrm{Re}\left\{ \begin{bmatrix} -C_1 m J_1(mR) - C_2 k J_1(\alpha R) \\ C_1 k J_0(mR) + C_2 \alpha J_0(\alpha R) \end{bmatrix} e^{i\omega t + kz} \right\}. \tag{15a,b}$$

Since $\cos(\omega t + k_i z)\, e^{k_r z}$ and $\sin(\omega t + k_i z)\, e^{k_r z}$ are linearly independent functions for all t and z, their respective coefficients must separately vanish. As the constants $C_1 = C_{1r} + iC_{1i}$ and $C_2 = C_{2r} + iC_{2i}$ are complex, this condition produces four linear, real, homogeneous algebraic equations in four unknowns: C_{1r}, C_{1i}, C_{2r} and C_{2i}. Writing these four real equations in their equivalent complex forms produces

$$\begin{bmatrix} mJ_1(mR) & kJ_1(\alpha R) \\ kJ_0(mR) & \alpha J_0(\alpha R) \end{bmatrix} \begin{bmatrix} C_1 \\ C_2 \end{bmatrix} = \begin{bmatrix} 0 \\ 0 \end{bmatrix}. \tag{16}$$

Since at least one of C_1 and C_2 is arbitrary, the determinant of the coefficient matrix must be zero, yielding the *dispersion relation* or *eigenvalue equation*

$$m\alpha \frac{J_1(mR)}{J_0(mR)} - k^2 \frac{J_1(\alpha R)}{J_0(\alpha R)} = 0, \tag{17}$$

which provides the relationship between the complex eigenvalue k and radian frequency ω.

3. Exact numerical calculation of the eigenvalues using the method of eigenvalleys

Given the parameters ω, ν and ν', the dispersion relation can be solved for all the eigenvalues. However, this task is not straightforward, for the equation is transcendental in the eigenvalue k, which generally is a complex number. A technique called the *method of eigenvalleys* has been developed for solving the dispersion equation (Scarton 1970, 1973). This method uses the positive semi-definiteness property of the complex modulus of the *auxiliary complex function* or *auxiliary equation*

$$E(k) = m(k)\,\alpha(k) \frac{J_1(m(k)\,R)}{J_0(m(k)\,R)} - k^2 \frac{J_1(\alpha(k)\,R)}{J_0(\alpha(k)\,R)}, \tag{18}$$

for $k = k_r + ik_i$ an *arbitrary* complex number. [$E(k)$ is the left-hand side of (17).]

† Because of axisymmetry and no axial swirl velocity, the vorticity has only a θ component Ω_θ.

Application of the method of eigenvalleys involves the computer calculation (Scarton 1970, 1971, 1973) and automatic computer plotting of logarithmic contours (Robinson & Scarton 1972) of the surface $|E(k_r, k_i)|$, called an *eigensurface*, over some predefined region of complex-k space. Since the only way a minimum of $|E(k)|$ can be obtained *inside* the region boundary is if $E(k)$ takes on the value zero (cf. the maximum modulus principle, Nehari 1965, pp. 142–144), *all* concave-upward regions will contain eigenvalues at their base; these concave-upward regions are called eigenvalleys. (In like manner, all concave-downward *interior* regions will contain singularities of $E(k)$.) The exact location of the base of each eigenvalley is then calculated numerically using minimization techniques. Details of the development of all computer programs used in the calculation, along with actual program listings, are contained in the dissertation by Scarton (1970).

All quantities are made dimensionless, as follows: frequency $F = \omega R/c_0$; first coefficient of viscosity $D = \nu/Rc_0$; second coefficient of viscosity $D' = \nu'/Rc_0$; propagation constant $\gamma = kR$; $M = mR$; $A = \alpha R$; $E(\gamma) = R^2E(k)$. Equations (7), (9) and (18) then become

$$E(\gamma) = MA\frac{J_1(M)}{J_0(M)} - \gamma^2\frac{J_1(A)}{J_0(A)}, \quad M = \left[\gamma^2 + \frac{F^2}{1+iF(D'+\frac{4}{3}D)}\right]^{\frac{1}{2}}, \quad A = \left[\gamma^2 - \frac{iF}{D}\right]^{\frac{1}{2}}.\dagger \tag{19a,b,c}$$

A summary of the range of parameters used in the study of the zeros of (19) is given in table 1. The values of the dimensionless first coefficient of viscosity D selected are 10^{-7}, 10^{-4} and 10^{-2}, which are defined as cases B, C and A, respectively. The values of the dimensionless frequency F selected vary *continuously* from well into the low-frequency range to well into the ultra-high-frequency range. The second coefficient of viscosity ν' (dimensionless form D') is assumed to be zero in this paper.‡

Using this technique, the co-ordinates of thirty-two eigenvalleys were identified and calculated to five-place accuracy, and are extensively tabulated by Scarton (1970).

† It is immediate that $A = 0$ is a zero of (19a); this produces the result (21) given later [cf. §4.2].

‡ The assumption of zero second coefficient of viscosity is justified, except at ultra-high frequency, by examining the factor $[1+iF(D'+\frac{4}{3}D)]$ of (19b), which is the *only* place where D' appears. Experimental data (Rosenhead 1954) indicate that

$$1{\cdot}7\nu \leqslant \nu' \leqslant 4{\cdot}7\nu.$$

Calculation of this factor for the largest values of F and D employed herein and ν' in the preceding range shows that the imaginary part of the factor is many orders of magnitude smaller than unity, except at ultra-high frequency, and thus negligible. Hence, the effects of boundary dissipation due to the zero speed at the wall very much dominate relaxation effects at frequencies small compared with the relaxation frequency; at ultra-high frequencies comparable with the relaxation frequency, the viscous and dilatational boundary layers at the wall are extremely thin owing to skin depth effects [to be discussed later, see §5], and the effect of setting D' to zero remains to be clarified. The thinness of the boundary layers in this latter case produces a situation that is very similar to the ultra-high-frequency acoustic propagation in a half-space, where relaxation effects are shown to be relevant (Lighthill 1956, §§3, 4).

Case	D	F	Liquid	R (in.)	f (Hz)
A	10^{-2}	0·01–50·0	Glycerine	0·0021	$53 \times 10^{+3}$–$265 \times 10^{+6}$
C	10^{-4}	0·0002–95	Water	0·00025	$7{\cdot}56 \times 10^{+3}$–$3{\cdot}6 \times 10^{+9}$
			Glycerine	0·21	$10{\cdot}6$–$5{\cdot}05 \times 10^{+6}$
B	10^{-7}	5×10^{-6}–0·01	Water	0·25	0·189–379

TABLE 1. Dimensionless first coefficient of viscosity D and dimensionless frequency range F with corresponding fluid equivalent, tube radius R, and cyclic frequency range f at room temperature (70 °F). [The dimensionless second coefficient of viscosity D' is zero for all cases studied. The above viscosity data are taken from Olson (1962, pp. 19–20).]

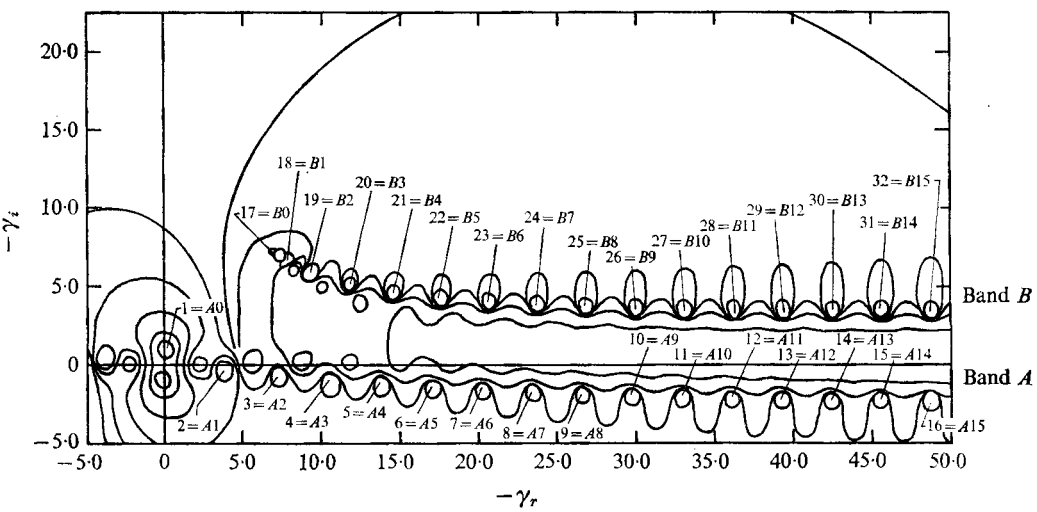

FIGURE 2. Main eigensurface. Case A: $F = 1{\cdot}0$, $D = 10^{-2}$ (eigenvalue numbering scheme defined).

4. Discussion of results of the complex eigenvalue calculation

4.1. *Examination of a representative eigensurface*

Figure 2 shows a typical eigensurface logarithmic contour plot ($F = 1{\cdot}0, D = 0{\cdot}01$, $D' = 0{\cdot}0$).† The changes in the locations of the eigenvalues γ with changes in frequency F, i.e. the *dispersive* behaviour of the eigenvalues, are seen by examining the eigenvalue trajectories for $D = 0{\cdot}01$ and $D' = 0$ in figure 3. The eigensurface plots reveal the existence of *two* bands of eigenvalues, called the A band and the B band. The A-band eigenvalues lie in quadrants I and IV near the real and imaginary axes; the B-band eigenvalues are contained entirely in quadrant I in the region between the real axis and a line through the origin at 45° to the real axis. (Only the first sixteen eigenvalues from each band are shown in the figures.) Both band A and band B have equivalent eigenvalues located in quadrants II and III. Because of symmetry about the origin ($E(\gamma)$ is an even function), the only difference between these eigenvalues and their quadrant I

† Notice that $(-\gamma_r, -\gamma_i)$ have been chosen as co-ordinates, and that references to quadrants I–IV refer to this co-ordinate system (e.g. the point $-\gamma_r = 2$, $-\gamma_i = 3$ lies in quadrant I).

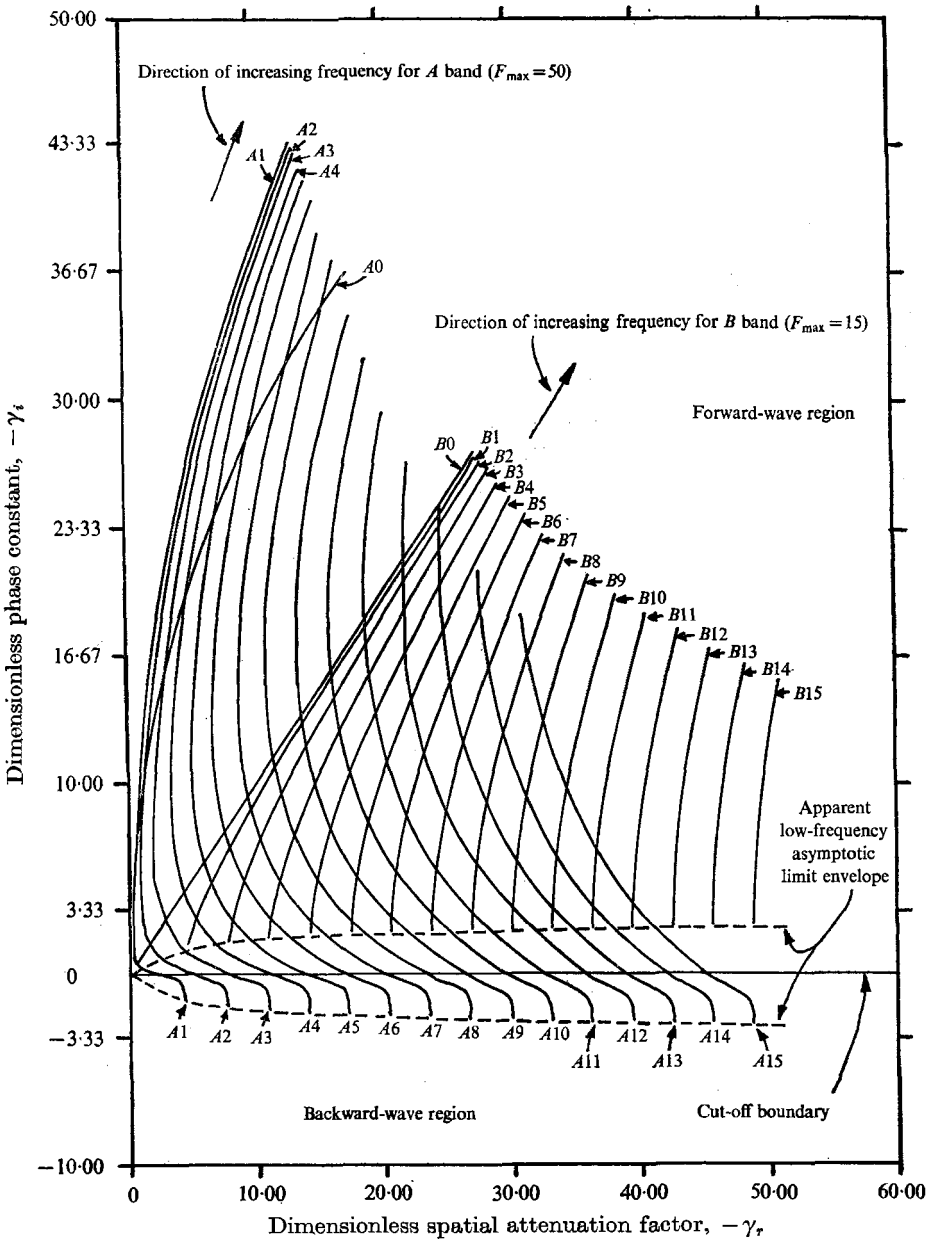

FIGURE 3. Eigenvalue trajectories. Case A: $D = 10^{-2}$, $D' = 0$.

and quadrant IV counterparts is that their signs are reversed. Located between the eigenvalues are isolated interior regions of high elevation. Of course, $E(k)$ is not analytic in these regions and its poles occur at the zeros of $J_0(M)$ and $J_0(A)$, which were artificially introduced in order to normalize the dispersion relation and, thus, avoid unreasonably large overall eigensurface heights away from the eigenvalleys.

The A band possesses a definite starting eigenvalue $A0$, which, for dimensionless

frequencies lower than one, is located very close to the origin and, for increasing dimensionless frequencies above one, proceeds up and to the right, with its dimensionless imaginary part approximately equal to the dimensionless frequency; the B band also possesses a definite starting eigenvalue $B0$, which, for F less than D, is within one unit of the origin and located on a line at 45° to the axes and, for increasing dimensionless frequencies above the dimensionless viscosity, moves farther out along the 45° line into the first quadrant. The higher A-band eigenvalues beginning with $A1$ are located on a concave-upward curve which starts at a position near $A0$, proceeds down and to the right, and eventually becomes uniformly spaced and parallel to the real axis lying some fixed distance below it; the higher B-band eigenvalues beginning with $B1$ are located on a curve passing through $B0$ which is concave downward at low frequencies and concave upward at high frequencies, and which proceeds from $B0$ to the right, eventually becoming uniformly spaced and parallel to the real axis, lying a fixed distance above it.† At dimensionless frequencies smaller than the dimensionless viscosity, the successive higher numbered eigenvalue pairs, $A1$ and $B1$, $A2$ and $B2$, and so forth, tend to be complex conjugates of each other. As the frequency is increased, the higher numbered A-band eigenvalues individually swing up and to the left, and then gradually to the right, $A0$ moving adjacent to successively higher numbered eigenvalues; the higher B-band eigenvalues individually move up and to the right and directly follow the trend set by $B0$.

Sample studies for other dimensionless viscosities in the wider range

$$10^{-8} \leqslant D \leqslant 10^{+1}$$

are given by Scarton (1970). These additional studies show that small viscosities keep the A-band eigenvalues very near to both the real and the imaginary axes, while higher viscosities allow the A-band eigenvalues to move farther away from the imaginary axis and to cross over the real axis more quickly; for the B band, small viscosities allow the eigenvalues to move away from the origin in quadrant I more rapidly than at the larger viscosities.

4.2. *The examination of dispersion curves*

Rewriting (5) in terms of dimensionless time $T = c_0 t/R$, axial co-ordinate $Z = z/R$, radial co-ordinate $\mathscr{R} = r/R$ and *wavelength* $\Lambda = \lambda/2\pi R = -1/\gamma_i$ gives

$$f^*(\mathscr{R}, Z, T) = \mathrm{Re}\{f^*(\mathscr{R}) \exp[i(FT - Z/\Lambda) + \gamma_r Z]\}, \tag{20}$$

where f^* refers to the dimensionless *eigenfunction* or *mode* f, the phase of f^* is given by the real quantity $FT + \gamma_i Z$, γ_i is known as the dimensionless *phase constant* and γ_r is called the *attenuation constant* or *spatial attenuation factor*. The dimensionless *phase velocity*, the velocity at which a point of constant modal phase $FT + \gamma_i Z$ advances, is $c_p^* = c_p/c_0 = -F/\gamma_i$. For an *inviscid* compressible liquid, the dimensionless *group velocity* $c_G^* = c_G/c_0 = -dF/d\gamma_i$ is the velocity at which the modal wave energy advances. For a *viscous*, and therefore dissipative, compressible liquid, the concept of group velocity, as defined by the above relation,

† An asymptotic equation for the large $|\gamma_{r_n}|$ eigenvalues is given at the end of §4.2.

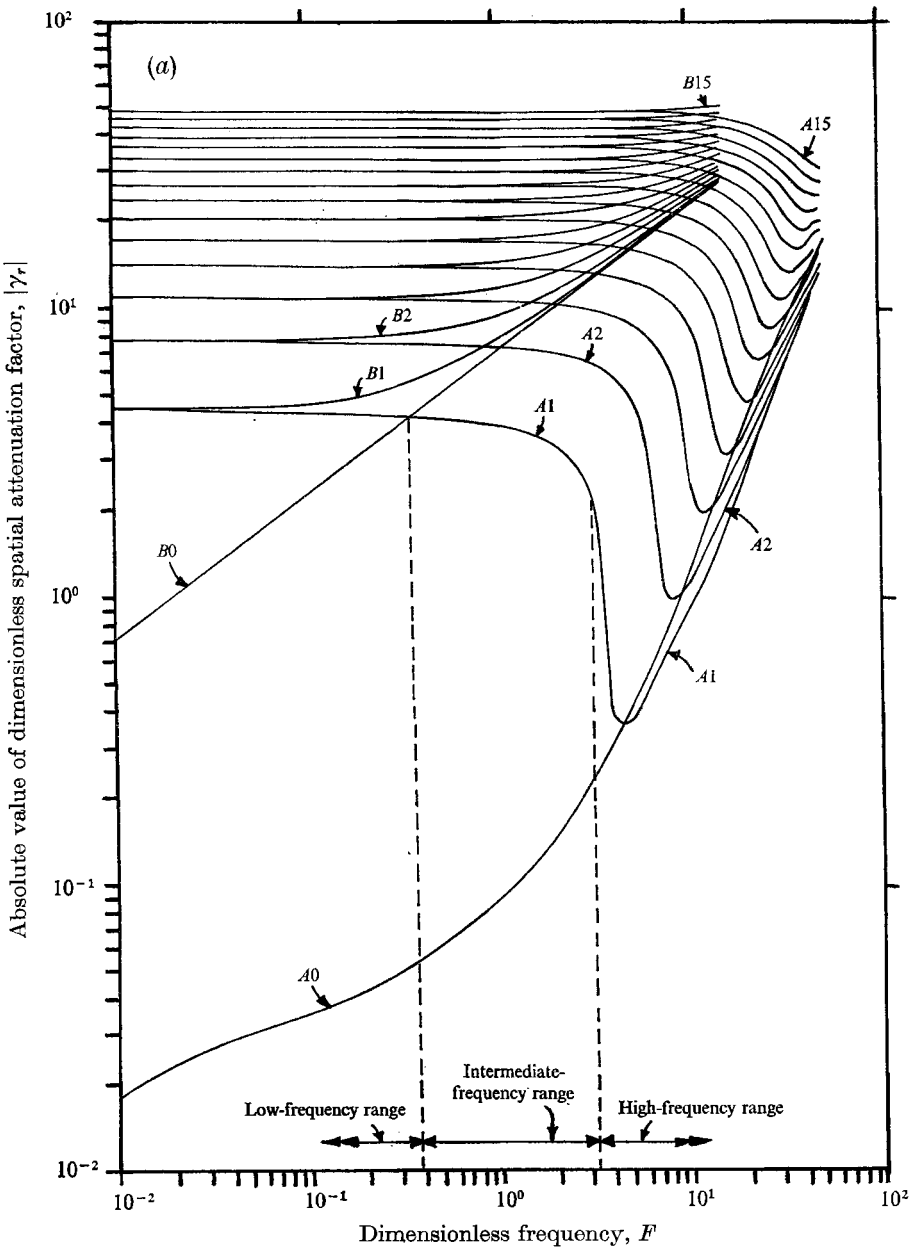

FIGURE 4(*a*). For legend see p. 605.

becomes ambiguous and can define velocity of modal energy only when $|\gamma_i| \gg |\gamma_r|$ (Lighthill 1965, § 3). When this inequality does not hold, the concept of group velocity must be replaced by the more general concept of a radiation condition obtained by evaluating the time-averaged flux of energy through the tube cross-section for a given mode. If the phase velocity and energy flux have the same sign, the mode is said to be a *forward* (*propagating*) *wave*; if the two have opposite signs, the affected mode is referred to as a *backward wave*.

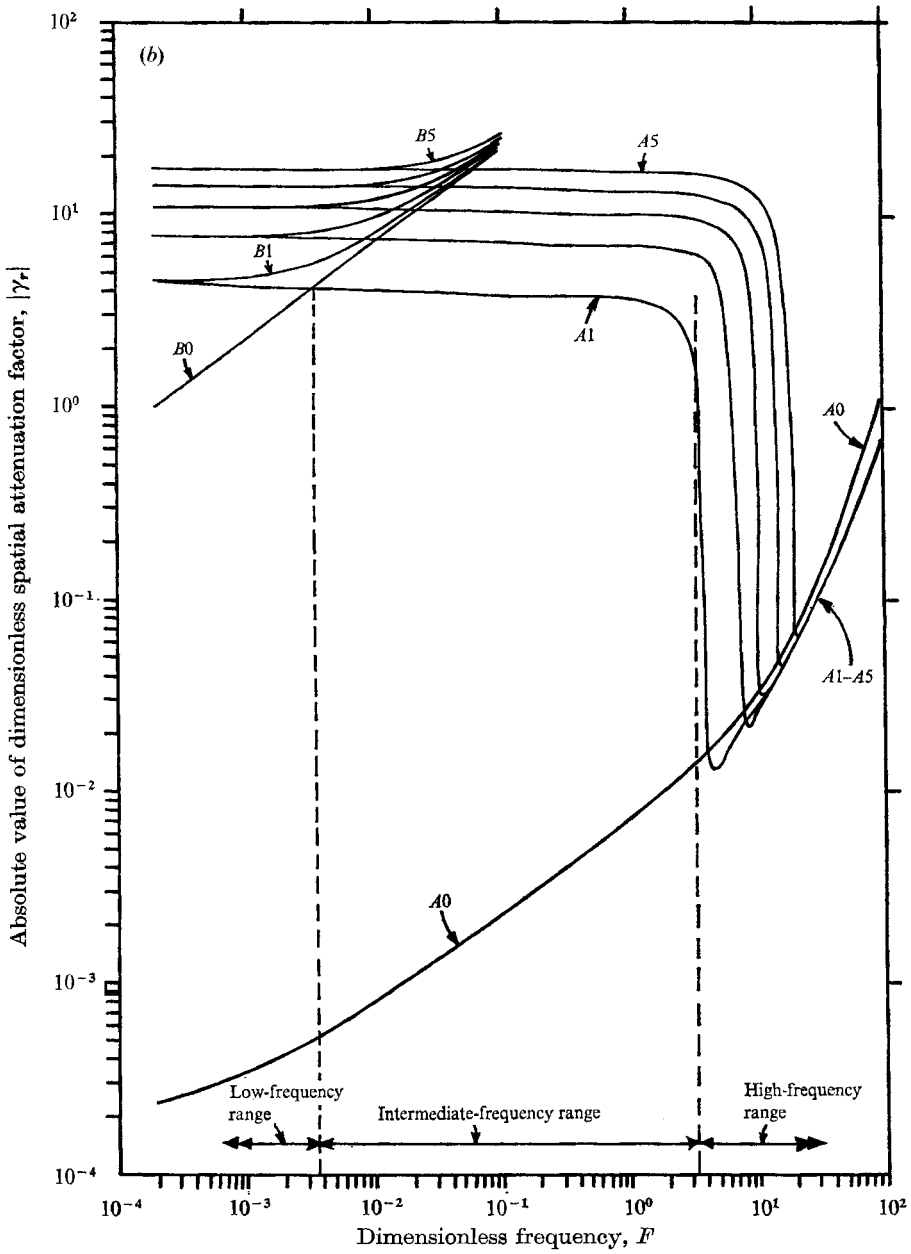

FIGURE 4 (*b*). For legend see facing page.

The dispersion curves plotted in figures 4 (*a*), (*b*) and (*c*) show the dependence of the attenuation constant γ_r on the dimensionless frequency F in quadrants I and IV. Since there is no internal energy source present (such as in a streaming liquid, where the zeroth-order solution would exchange energy with the first-order solution), the typical source of modal excitation (such as an oscillating piston) is discretely located at some specified axial position, and the viscous fluid is dissipative, these quadrant I and IV eigenvalues with negative attenuation con-

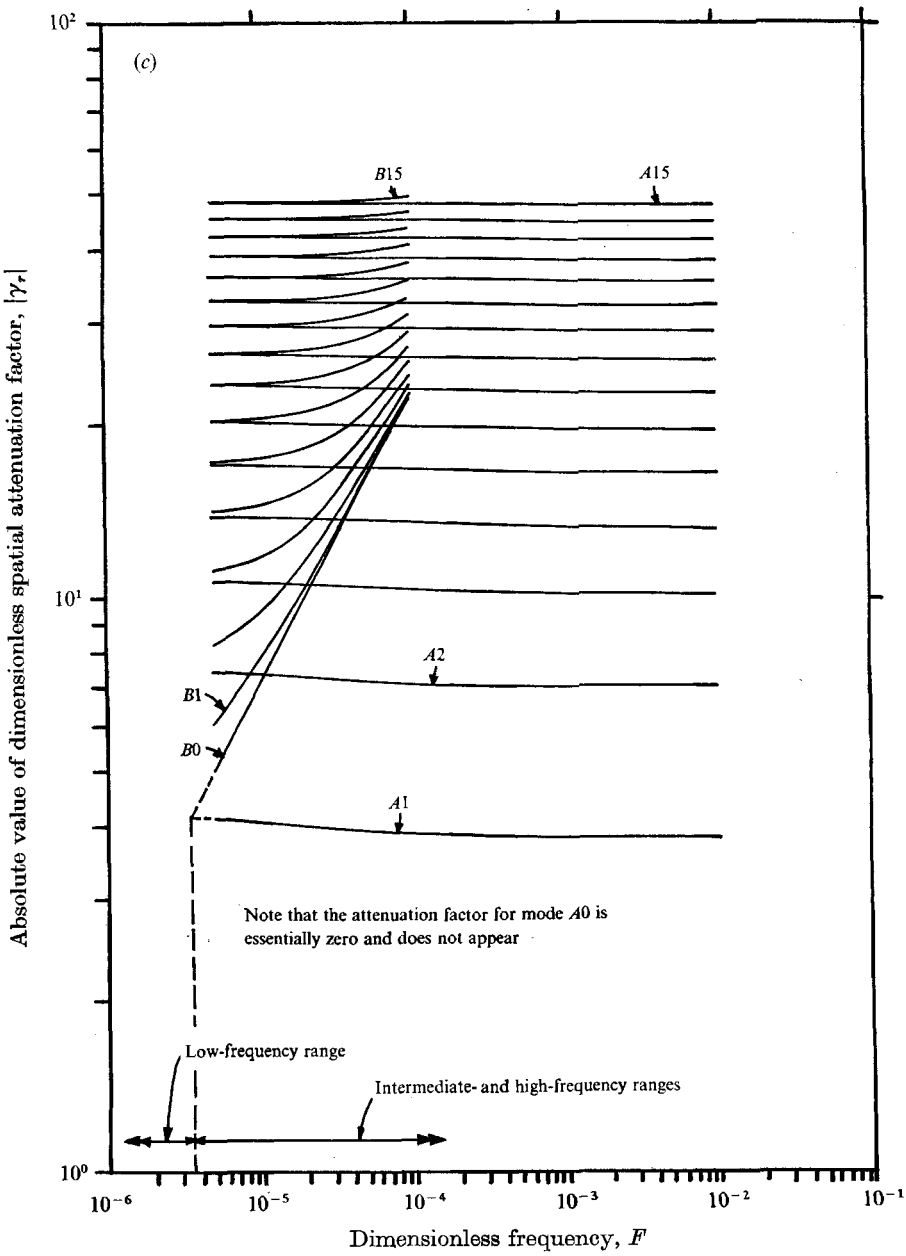

FIGURE 4. Spatial attenuation factor dispersion curves with all $\gamma_r < 0$. (*a*) Case *A*: $D = 10^{-2}$, $D' = 0$. (*b*) Case *C*: $D = 10^{-4}$, $D' = 0$. (*c*) Case *B*: $D = 10^{-7}$, $D' = 0$. (γ_{rA0} for case *B* is essentially zero.)

stants must be associated with the positive radiation of energy. By the same argument the quadrant II and III eigenvalues with positive attenuation constants are associated with a negative radiation condition. Also, examination of the eigenvalues close to the imaginary axis (where $|\gamma_i| \gg |\gamma_r|$, so that the group velocity $c_G^* \approx -dF/d\gamma_i$ is a valid concept) tends to confirm the argument.

Comparison of the attenuation constant dispersion plots for the three cases reveals that a distinct boundary between low-frequency and intermediate-frequency behaviour can be defined as that frequency, denoted by F_{LI}, where the $A1$ and $B0$ attenuation constants are equal. The low-frequency region is found below F_{LI} and is where the $A0$ and $B0$ modes attenuate at rates much smaller than those for all other modes and higher numbered pairs AN and BN ($N \geqslant 1$) are very nearly complex conjugates of each other. The intermediate- and high-frequency ranges occur above F_{LI} and are where the $A0$ and $A1$ modes (and for frequency high enough, successively higher numbered A-band modes) attenuate at spatial rates much smaller than those for all other modes. Hence, this definitive low–intermediate dimensionless frequency boundary F_{LI} provides a means of determining the relative importance of the A and B bands. For dimensionless frequencies below F_{LI}, the A band and B band have the same importance, since their respective modes decay spatially at approximately the same rate; for dimensionless frequencies above F_{LI}, the A band becomes much more important than the B band, since each lower numbered B-band mode decays spatially many times more rapidly than its counterpart on the A band. For cases A, C and B, the respective approximate dimensionless low–intermediate frequency boundaries F_{LI} are 0·35, $3{\cdot}55 \times 10^{-3}$ and $3{\cdot}51 \times 10^{-6}$.

Lighthill (1970, private communication) has observed that the low–intermediate boundary always seems to occur when $F/D \approx O(10)$. Based on this observation and the extensive parameter coverage by Scarton (1970), it has been found that F_{LI} can be written empirically as $11{\cdot}14\pi D$. (The slight variation in the case B data was ignored in the calculation, since it is based on an extrapolation.)

Dispersion curves showing the dimensionless phase velocity c_p^* as a function of the dimensionless frequency F are plotted in figures 5 (a), (b) and (c).† Notice that the $A0$ and all of the B-band phase velocities are positive for all frequencies, but that, depending on frequency, the $A1$ and higher numbered A-band phase velocities may be positive or negative. Since the radiation condition is positive for all quadrant I and IV eigenvalues, the $A0$ mode and all B-band modes are forward waves, while the $A1$ and higher numbered A-band modes can either be backward, for low enough frequency, or forward propagating, for the higher frequencies.

Since the dimensionless wavelength Λ is the negative reciprocal of the dimensionless phase constant γ_i, the phase constant plots (Scarton 1970) show that the dimensionless wavelength for the modes varies *continuously* over a very large range, encompassing magnitudes much larger than one for low frequencies and magnitudes much smaller than one for high frequencies. For case C, this wavelength variation for the mode $A0$ extends from the very long Λ of 3000 for $F = 0{\cdot}0002$ to the very short Λ of 0·0105 for $F = 95{\cdot}0$.

Comparison of the phase-velocity dispersion plots reveals that a distinct boundary between intermediate- and high-frequency modal behaviour can be defined as that frequency F_{IH} for which the $A1$ phase constant equals zero. Above F_{IH}, the phase of mode $A1$ propagates in the positive direction, while below F_{IH} it propagates in the negative direction. Also, below F_{IH} mode $A0$

† The corresponding phase constant γ_i versus dimensionless frequency F dispersion plots are given by Scarton (1970).

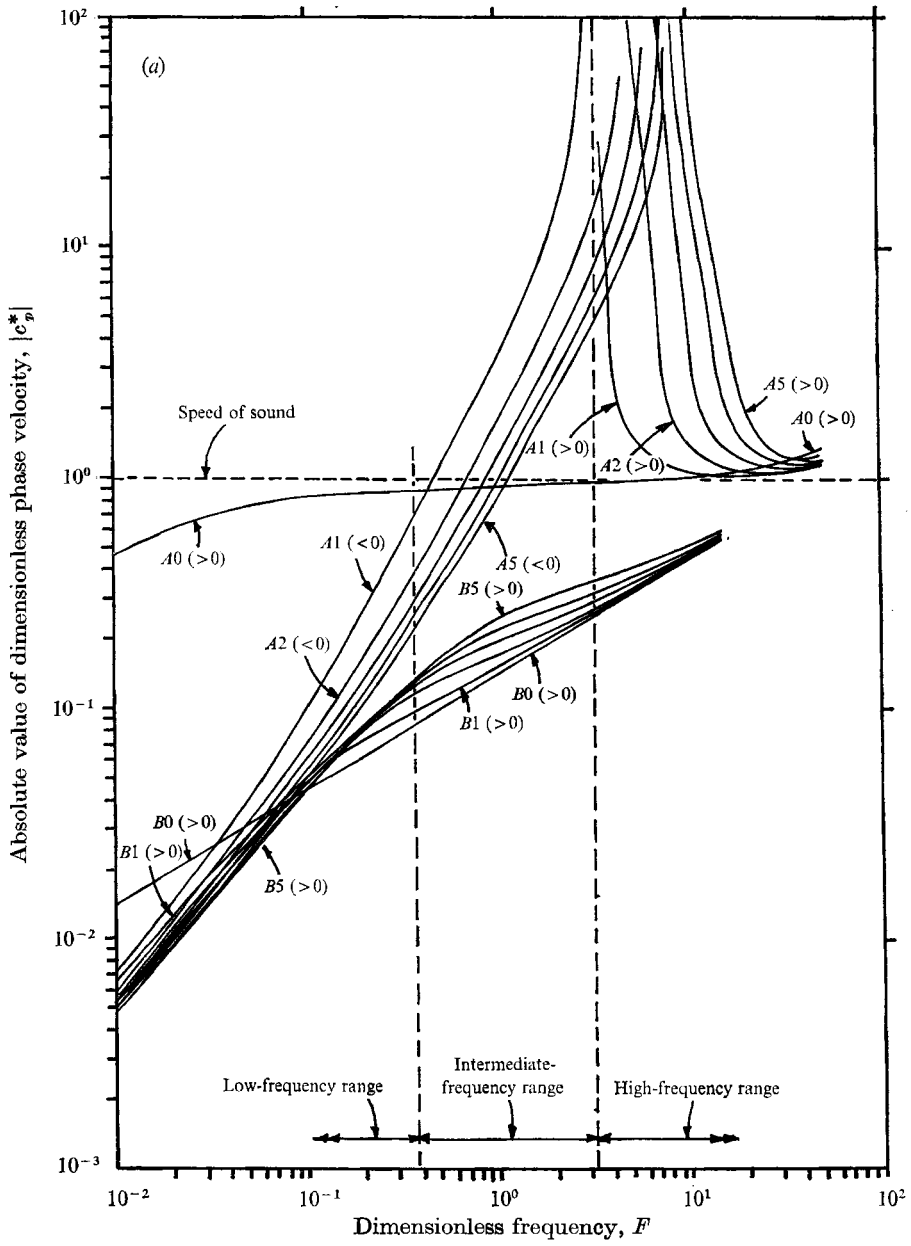

FIGURE 5(*a*). For legend see p. 608.

has a very small attenuation constant compared with those of the other A-band modes (which, in contrast to mode $A0$, are backward propagating below F_{IH}). For frequencies somewhat higher than F_{IH}, mode $A1$ and higher modes have attenuation constants that are slightly less than the value for mode $A0$.

In cases A and C, F_{IH} is very nearly π at the approximate value 3·1 for $10^{-2} \geqslant D \geqslant 10^{-4}$, so that the width of the intermediate frequency range F_{IH}/F_{LI} is given by $0{\cdot}089/D$.

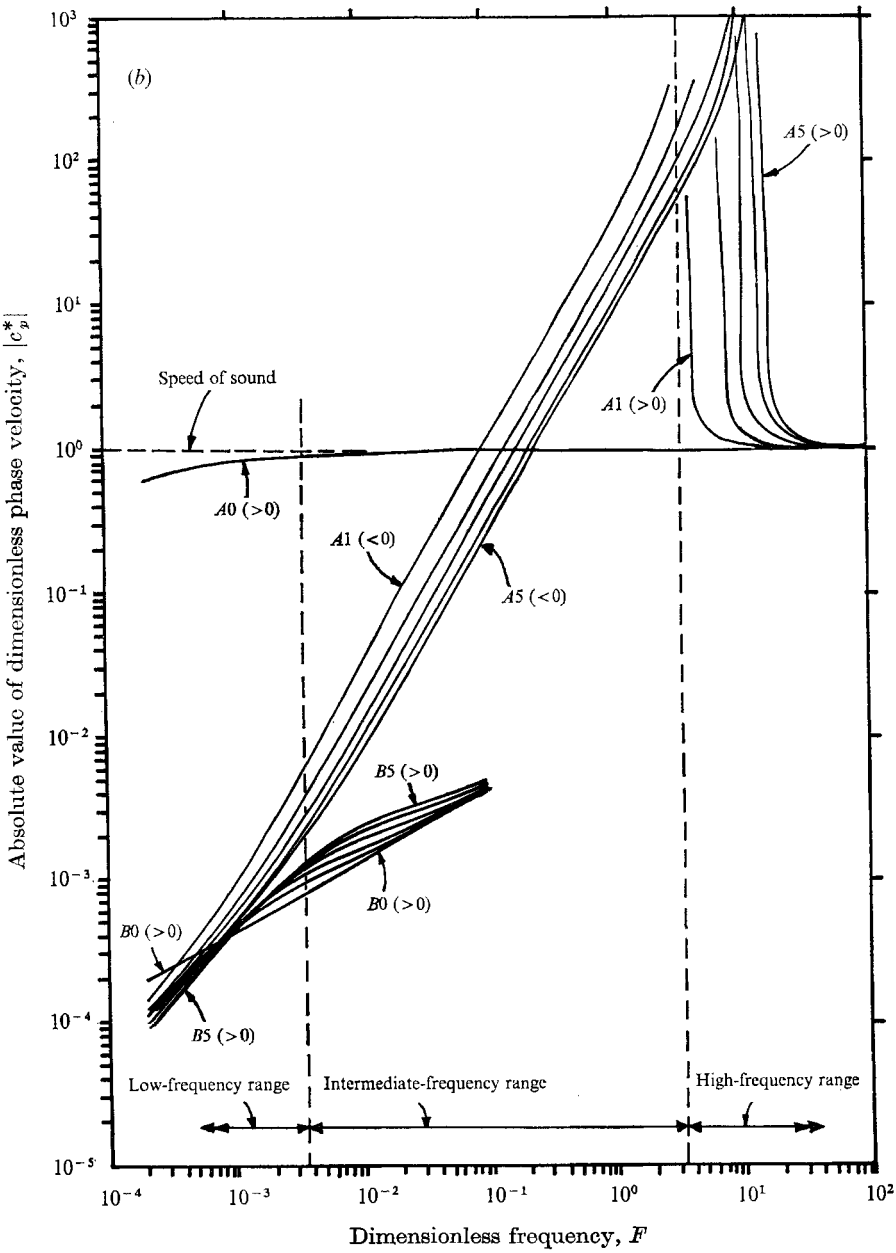

FIGURE 5(*b*). For legend see facing page.

Examination of the dispersion curves (figures 4, 5) shows that the real and imaginary parts of the eigenvalue γ_{B0} are equal and proportional to $(F/D)^{\frac{1}{2}}$. From the figures it is found that

$$\gamma_{B0} = \mp (F/2D)^{\frac{1}{2}}(1+i), \tag{21}$$

which is an exact zero of the auxiliary equation (19) for arbitrary F and D, and for all D' as well. The mode $B0$ dimensionless phase velocity is $c^*_{pB0} = \pm (2DF)^{\frac{1}{2}}$. (The concept of group velocity does not apply, since $\gamma_r = \gamma_i$.)

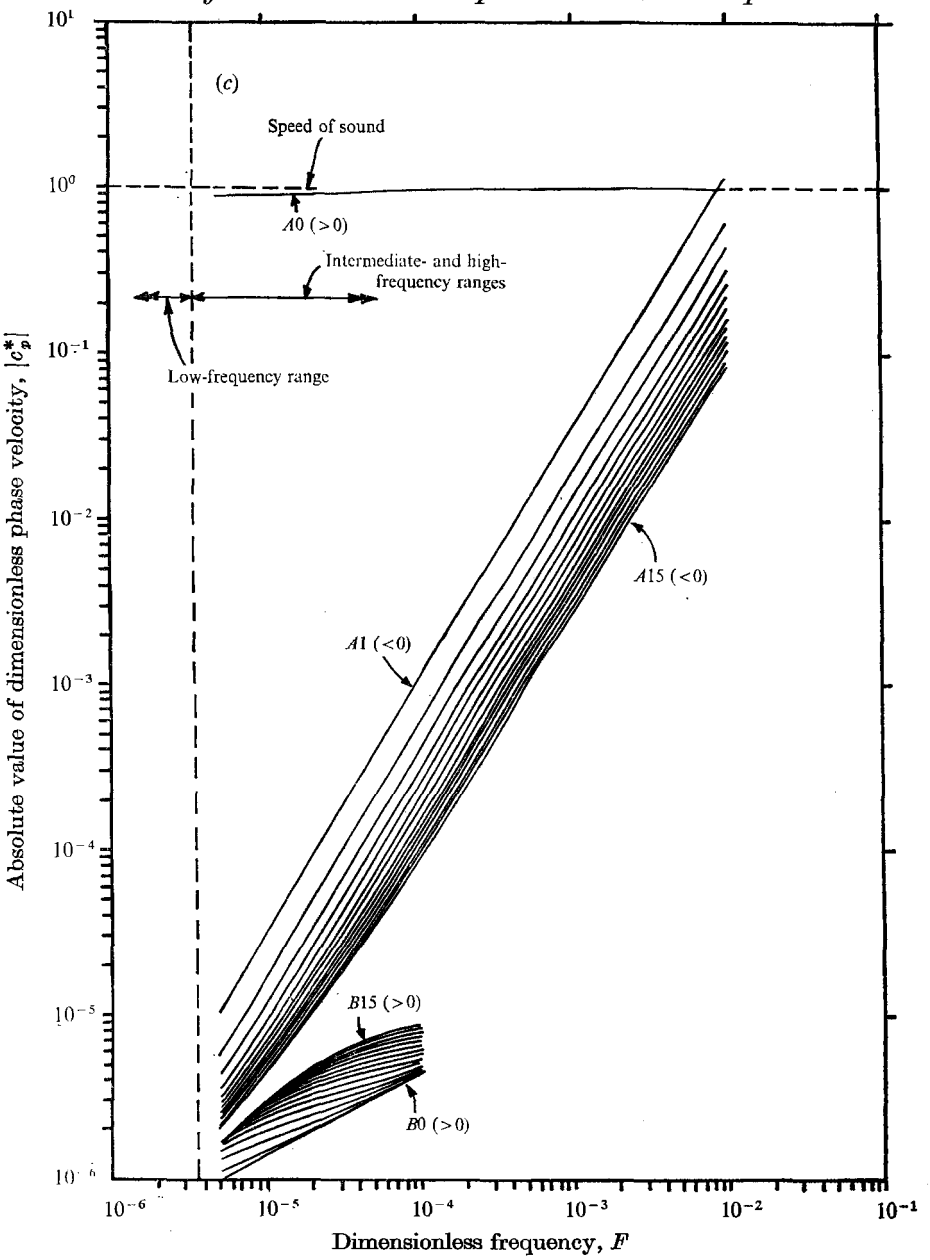

FIGURE 5. Phase-velocity dispersion curves. (*a*) Case A: $D = 10^{-2}$, $D' = 0$. (*b*) Case C: $D = 10^{-4}$, $D' = 0$. (*c*) Case B: $D = 10^{-7}$, $D' = 0$.

Equation (21) shows that $\gamma_{B0} = 0$ for zero frequency. An analytical expression for γ_{A0} has been given by Brown (1962) for small viscosity, and this shows that γ_{A0} is zero for zero frequency. These limits are also evident upon extrapolating the $A0$ and $B0$ eigenvalue trajectories in figure 3. Fitz-Gerald (1969, 1972) shows the same eigenvalue behaviour, but in a different way; by ignoring compressibility and inertial effects entirely in deriving his eigenvalue equation he has,

in effect, taken the zero-frequency limit *a priori* and has found the trivial eigenvalue $\gamma = 0$. Thus, a condition of modal degeneracy exists at zero frequency, with $\gamma_{A0}(F = 0) = \gamma_{B0}(F = 0) = 0$. Comparison with the non-viscous compressible eigenvalue is instructive. In § 5 it will be shown that the A-band eigenvalues are the viscous equivalents of the non-viscous eigenvalues. The lowest non-viscous eigenvalue is γ_0, and $\gamma_0 = \pm F$, which vanishes for zero frequency, exhibiting the same degeneracy as the corresponding viscous mode γ_{A0}.

The limiting solution for the low-frequency complex conjugate behaviour exhibited by the higher numbered A- and B-band eigenvalues is contained in the work by Fitz-Gerald through the solution of the zero-frequency dispersion equation $\gamma[J_0^2(\gamma) + J_1^2(\gamma)] = 2J_0(\gamma)J_1(\gamma)$. (This expression is easily obtained from (17) by taking the zero-frequency limit of (17) expanded in Taylor series about zero frequency.) Fitz-Gerald gives the asymptotic form of higher numbered eigenvalues as $\gamma_n = \mp\frac{1}{2}(2n+1)\pi \pm i \ln[(4n+2)\pi]$ (for large n).† Fitz-Gerald has tabulated the values of the first ten eigenvalues; they agree very well with the low-frequency eigenvalues tabulated by Scarton (1970) (as well as with the higher frequency eigenvalues, for n large enough).

Onoe, McNiven & Mindlin (1962) have obtained zero-frequency results that are qualitatively similar to this limit in their solution of axially symmetric waves in an infinitely long, isotropic, circular, non-dissipative rod, as given by Pochhammer's equation: they describe a spectrum, covering a large range of real frequencies, which includes real, imaginary and complex propagation constants. Contrary to the viscous-fluid eigenvalues, regardless of frequency the Onoe *et al.* eigenvalues always appear in complex conjugate pairs owing to their elastic and therefore conservative nature.

5. Radial mode structure

5.1. *Calculation of the field quantities*

Expressions for the dimensionless radial and axial velocity are obtained by writing the constant C_2 in terms of C_1. From (15a, b) these are in dimensionless form

$$C_{2n}^* = -\frac{M_n J_1(M_n)}{\gamma_n J_1(A_n)} C_{1n}^* = -\frac{\gamma_n J_0(M_n)}{A_n J_0(A_n)} C_{1n}^*, \tag{22}$$

where $C_{1n}^* = C_{1n}/Rc_0$, $C_{2n}^* = C_{2n}/Rc_0$ and n refers to the nth mode. The dimensionless modal solutions for radial and axial velocity from (10), (11) and (22) become

$$\begin{bmatrix} V_{rn}^* \\ V_{zn}^* \end{bmatrix} = \mathrm{Re}\left\{ C_{1n}^* \begin{bmatrix} M_n J_1(M_n)\left[-\dfrac{J_1(M_n\mathscr{R})}{J_1(M_n)} + \dfrac{J_1(A_n\mathscr{R})}{J_1(A_n)}\right] \\ \gamma_n J_0(M_n)\left[\dfrac{J_0(M_n\mathscr{R})}{J_0(M_n)} - \dfrac{J_0(A_n\mathscr{R})}{J_0(A_n)}\right] \end{bmatrix} \exp(iFT + \gamma_n Z) \right\} \tag{23}$$

respectively, where $V_{rn}^* = v_{rn}/c_0$ and $V_{zn}^* = v_{zn}/c_0$. Modal solutions for the dimensionless perturbation pressure, scalar potential, perturbation density, θ com-

† The four alternative choices of sign have been added to Fitz-Gerald's original expression, which showed only positive signs.

ponent of the vector potential and θ component of the vector vorticity from (12), (6), (13), (8) and (14) become

$$\begin{bmatrix} p_n^* \\ \phi_n^* \\ \rho_n^* \\ \psi_{\theta n}^* \\ \Omega_{\theta n}^* \end{bmatrix} = \mathrm{Re}\left\{ \begin{bmatrix} \begin{bmatrix} C_{3n}^* \\ C_{1n}^* \\ C_{3n}^* \end{bmatrix} J_0(M_n \mathscr{R}) \\ \begin{bmatrix} C_{2n}^* \\ C_{4n}^* \end{bmatrix} J_1(A_n \mathscr{R}) \end{bmatrix} \exp(iFT + \gamma_n Z) \right\} \tag{24}$$

respectively, where

$$p_n^* = p_n/\rho_0 c_0^2, \quad \phi_n^* = \phi_n/Rc_0, \quad \rho_n^* = \rho_n/\rho_0, \quad \psi_{\theta n}^* = \psi_{\theta n}/Rc_0,$$
$$\Omega_{\theta n}^* = R\Omega_{\theta n}/c_0, \quad C_{3n}^* = C_{3n}/\rho_0 c_0^2, \quad C_{4n}^* = RC_{4n}/c_0.$$

The modal equations (23) and (24) have the form

$$f_n^*(\mathscr{R}, Z, T; F, D) = \mathrm{Re}\{C_n^* g_n^*(\mathscr{R}; F, D) \exp(iFT + \gamma_n Z)\}$$

and are most concisely represented by plotting the real and imaginary parts of the radial eigenfunction g_n^*, normalized respectively by the maximum magnitude of the real or imaginary parts on the interval $0 \leqslant \mathscr{R} \leqslant 1$.

Two typical sets of plots (figures 6, 7) display the radial component of velocity V_{rn}^*, the axial component of velocity V_{zn}^*, the perturbation pressure p_n^* and the θ component $\Omega_{\theta n}^*$ of the vorticity for modes $A0$, $A1$, $A15$, $B0$, $B1$ and $B15$. Equation (24) shows that radial variations of ϕ_n^* and ρ_n^* are the same as those of p_n^*; likewise, the radial variation $\psi_{\theta n}^*$ is the same as that of $\Omega_{\theta n}^*$.

The first set of plots for $F = 0{\cdot}01$ and $D = 0{\cdot}01$ (figure 6) exhibits characteristic low-frequency behaviour ($F < F_{LI}$); the second set for $F = 0{\cdot}1$ and $D = 0{\cdot}0001$ (figure 7) exhibits characteristic intermediate–high-frequency behaviour ($F > F_{LI}$). A much expanded version of these plots is given by Scarton (1970). Some of the conclusions drawn here will be based on that expanded set of mode plots. The maximum magnitudes of the real and imaginary parts appear in table 2. (All plots are based on quadrant II and III eigenvalues; cf. § 4.1.)

5.2. *Verification of the modal no-slip condition and establishment of the essential physical mechanism which governs each mode*

The rigid impermeable wall boundary condition $v_r(R) = 0$ is seen to be satisfied for all modes in all cases. The no-slip condition $v_z(R) = 0$ is also satisfied for all modes, except apparently for the imaginary part of the axial velocity of mode $A0$ at high frequencies. However, since the no-slip and rigid impermeable wall boundary conditions are satisfied at lower frequencies for mode $A0$ (proving that $A0$ is in fact a mode), and since the $A0$ eigenvalley trajectory has been continuously followed for increasing frequency, the conclusion is that the apparent slip velocity is the result of a slight inaccuracy in eigenvalue $A0$ at these higher frequencies.

Mode plots for band A and band B show that the modal character for each band is fundamentally different. When the pressure and vorticity are examined for the intermediate–high-frequency case ($F = 0{\cdot}1$ and $D = 0{\cdot}0001$, figure 7), this difference is clearly demonstrated. In this case, the vorticity for the A band

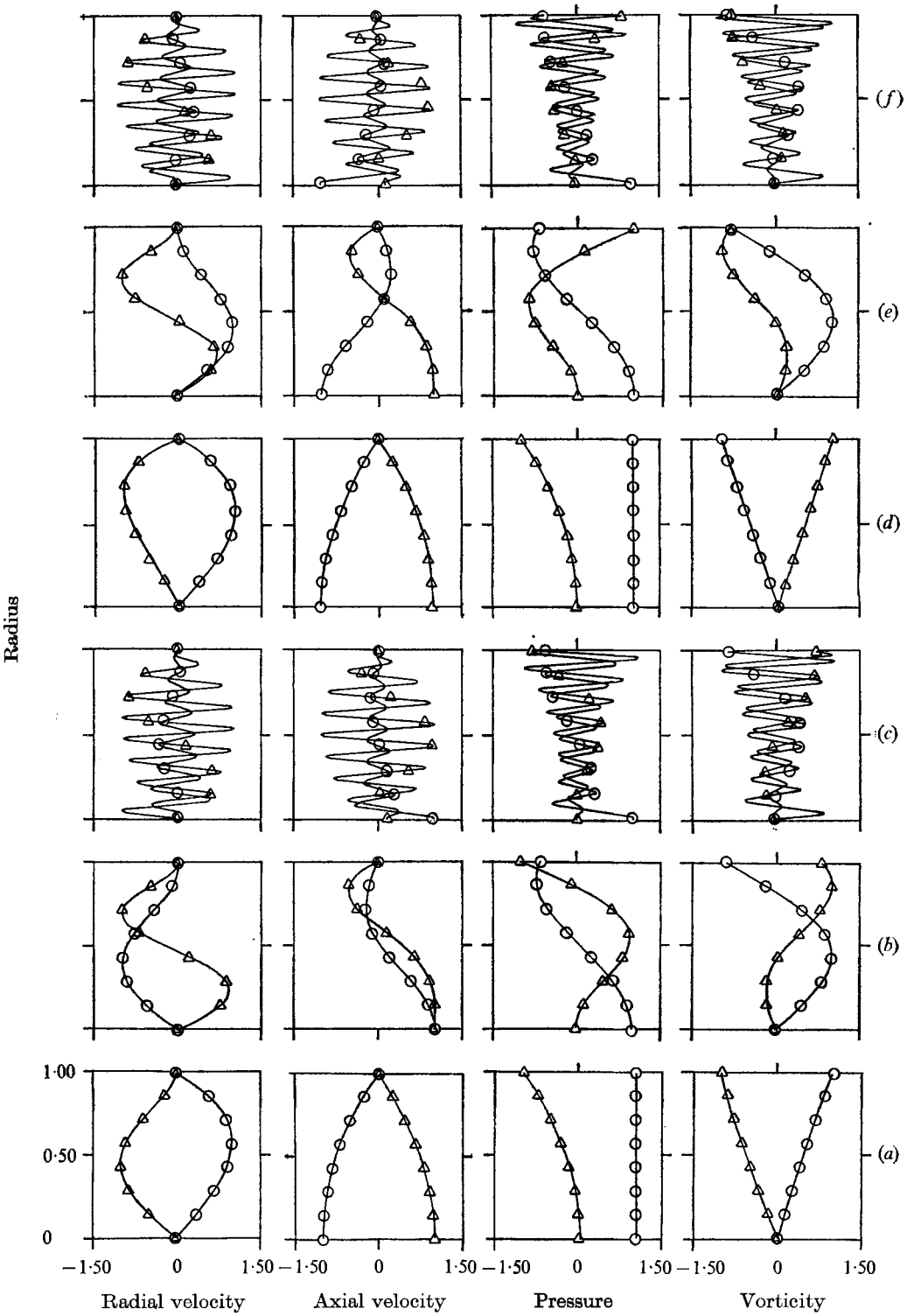

FIGURE 6. Radial mode structure for $F = 10^{-2}$ and $D = 10^{-2}$ (case A). ○, real part; △, imaginary part. The quadrant II and III eigenvalues are used. (*a*) Mode $A0$. (*b*) Mode $A1$. (*c*) Mode $A15$. (*d*) Mode $B0$. (*e*) Mode $B1$. (*f*) Mode $B15$.

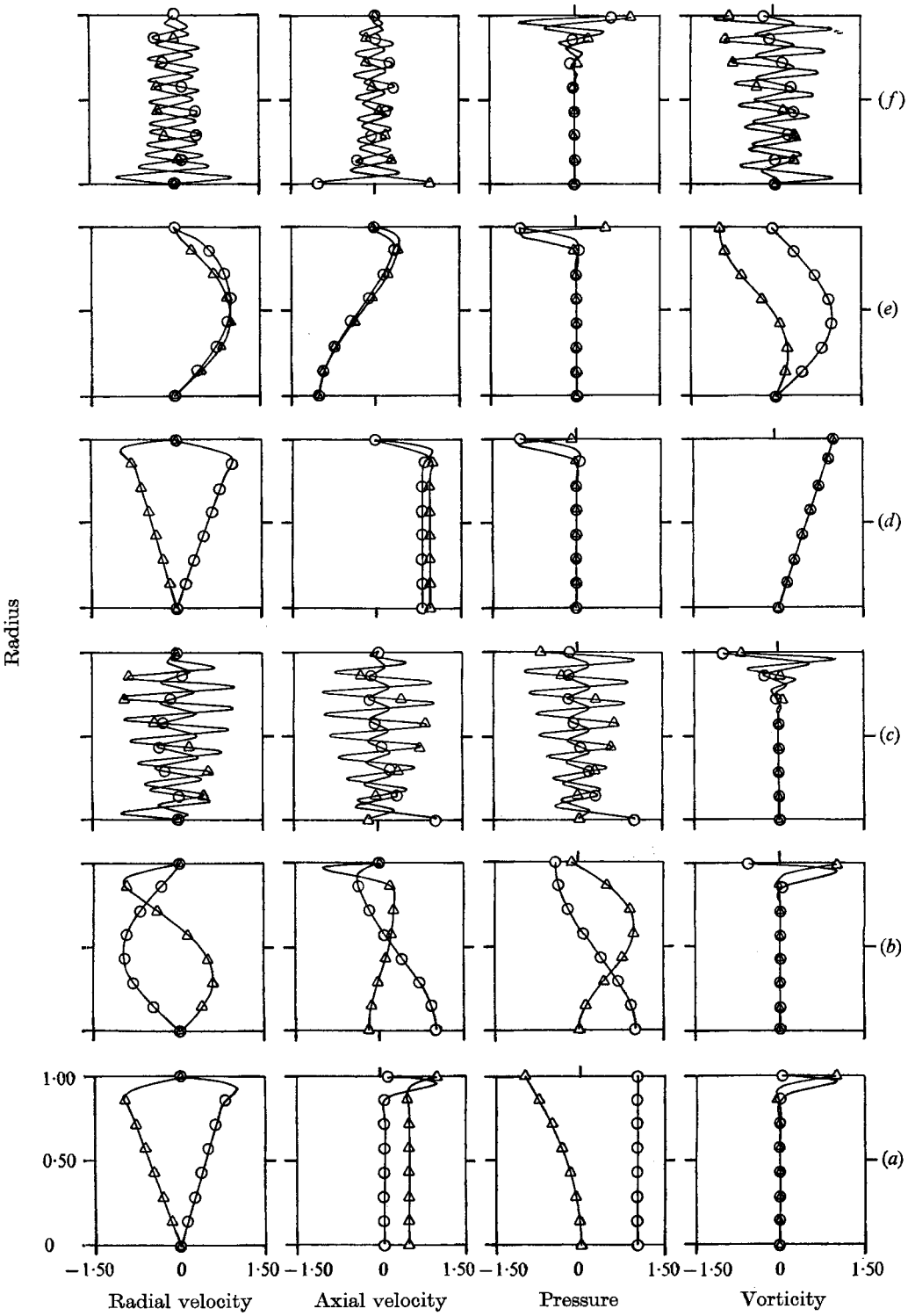

FIGURE 7. Radial mode structure for $F = 10^{-1}$ and $D = 10^{-4}$ (case C). ○, real part; △, imaginary part. The quadrant II and III eigenvalues are used. (*a*) Mode $A0$. (*b*) Mode $A1$. (*c*) Mode $A15$. (*d*) Mode $B0$. (*e*) Mode $B1$. (*f*) Mode $B15$.

Mode	max $\lvert V^*_{rr}\rvert$	max $\lvert V^*_{ri}\rvert$	max $\lvert V^*_{zr}\rvert$	max $\lvert V^*_{zi}\rvert$	max $\lvert p^*_r\rvert$	max $\lvert p^*_i\rvert$	max $\lvert \Omega^*_{\theta r}\rvert$	max $\lvert \Omega^*_{\theta i}\rvert$
				$F = 0{\cdot}01$ and $D = 0{\cdot}01$; figure 6				
$A0$	$0{\cdot}192-4$	$0{\cdot}605-6$	$0{\cdot}442-2$	$0{\cdot}545-2$	$0{\cdot}100+1$	$0{\cdot}200-3$	$0{\cdot}395$	$0{\cdot}307$
$A1$	$0{\cdot}255$	$0{\cdot}203-1$	$0{\cdot}437$	$0{\cdot}830-1$	$0{\cdot}100+1$	$0{\cdot}499$	$0{\cdot}671$	$0{\cdot}650$
$A15$	$0{\cdot}288$	$0{\cdot}587-1$	$0{\cdot}497$	$0{\cdot}589-1$	$0{\cdot}100+1$	$0{\cdot}668$	$0{\cdot}679$	$0{\cdot}751$
$B0$	$0{\cdot}240-1$	$0{\cdot}140-2$	$0{\cdot}165$	$0{\cdot}187$	$0{\cdot}100+1$	$0{\cdot}250$	$0{\cdot}307$†	$0{\cdot}396$†
$B1$	$0{\cdot}286$	$0{\cdot}245-1$	$0{\cdot}479$	$0{\cdot}107$	$0{\cdot}100+1$	$0{\cdot}524$	$0{\cdot}660$	$0{\cdot}597$
$B15$	$0{\cdot}291$	$0{\cdot}593-1$	$0{\cdot}502$	$0{\cdot}595-1$	$0{\cdot}100+1$	$0{\cdot}674$	$0{\cdot}673$	$0{\cdot}743$
				$F = 0{\cdot}1$ and $D = 0{\cdot}0001$; figure 7				
$A0$	$0{\cdot}258-3$	$0{\cdot}219-3$	$0{\cdot}362-1$	$0{\cdot}204$	$0{\cdot}100+1$	$0{\cdot}119-3$	$0{\cdot}119+9$	$0{\cdot}362+9$
$A1$	$0{\cdot}228+1$	$0{\cdot}121$	$0{\cdot}392+1$	$0{\cdot}480$	$0{\cdot}100+1$	$0{\cdot}286-1$	$0{\cdot}870+8$	$0{\cdot}303+9$
$A15$	$0{\cdot}282+2$	$0{\cdot}538+1$	$0{\cdot}486+2$	$0{\cdot}561+1$	$0{\cdot}100+1$	$0{\cdot}149$	$0{\cdot}350+4$	$0{\cdot}254+4$
$B0$	$0{\cdot}750+10$	$0{\cdot}915+10$	$0{\cdot}969+10$	$0{\cdot}878+10$	$0{\cdot}366+9$	$0{\cdot}121+9$	$0{\cdot}362+12$†	$0{\cdot}524+10$†
$B1$	$0{\cdot}221+11$	$0{\cdot}113+12$	$0{\cdot}196+11$	$0{\cdot}145+11$	$0{\cdot}307+9$	$0{\cdot}891+8$	$0{\cdot}582$	$0{\cdot}354-1$
$B15$	$0{\cdot}336+6$	$0{\cdot}561+6$	$0{\cdot}364+6$	$0{\cdot}101+7$	$0{\cdot}254+4$	$0{\cdot}352+4$	$0{\cdot}580$	$0{\cdot}151$

† $\Omega^*_{\theta B0}$ is computed using (25).

TABLE 2. Mode plot maximum magnitudes ($0 \leqslant \mathscr{R} \leqslant 1$).

(and the pressure for the B band) away from the tube wall is very much smaller than the vorticity for the A band (and pressure for the B band) adjacent to the tube wall; while, on the other hand, the pressure for the A band (and the vorticity for the B band) is generally not zero for any arbitrary radius. Thus, band A may be described as pressure-dominated (or dilatation-dominated), and band B as vorticity-dominated (or rotation-dominated).

5.3. *Study of the A-band modal structure*

The pressure dominance in the A band can be further illustrated by comparing its modes with the solution of the inviscid, compressible, rigid, impermeable tube dispersion relation $J_1(M_n) = 0$, where γ_n is obtained from (19) upon setting $D = D' = 0$ (cf. Redwood 1960). For the inviscid problem, γ_n is pure imaginary when $F > M_n$ and represents a state of non-attenuated propagation of longitudinal pressure waves; for $F < M_n$, γ_n is pure real and represents a state of pure diffusion (or evanescence); for the transition condition $F = M_n$, γ_n is zero and represents modal *cut-off*. Examination of high-frequency eigensurfaces (Scarton 1970) reveals similar behaviour for the A band, with the eigenvalues shown being nearly pure real or pure imaginary. Evidently, the A-band eigenvalues are the viscous equivalents of the zeros for the inviscid compressible solution, so that the A-band modes are excited primarily by an axisymmetric normal oscillation of the axisymmetric surface mentioned in § 2. If the oscillating disturbing surface were a flat axially oscillating piston, longitudinal dilatational pressure waves propagating in the Z direction would be generated.

Further, from figure 5(*b*), for example, the dimensionless $A0$ phase velocity is nearly equal to the inviscid zeroth-mode phase velocity (unity) for frequencies $F > F_{LI}$. For viscous modes AN ($N \geqslant 1$) the phase velocity approaches infinity (or $\gamma_i \to 0$) at values of F nearly equal to the cut-off frequencies of the corresponding inviscid modes (i.e. $F = 3{\cdot}83$, $7{\cdot}01$, $10{\cdot}2$, etc.). There is *no* cut-off for these viscous modes, but rather a transition from backward to forward waves, where, for the higher A-band modes, the dramatic drop in $|\gamma_r|$ (cf. § 4.2) occurs at the transition frequency for that mode.

Additional comparisons can be made on the basis of complex radial pressure variations. The inviscid pressure plots are given by Redwood (1960, p. 76) and for the zeroth mode show that the pressure is constant and pure real (i.e. a plane wave) for all frequencies. Comparison with the viscous mode $A0$ shows that for low viscosities and frequencies (figures 6*a*, 7*a*) the real part of the pressure is constant and the imaginary part has a comparatively small magnitude, so that there is a close correspondence with the inviscid plane wave. However, for higher frequencies and viscosities, both real and imaginary parts of the pressure vary with radius and thus the $A0$ mode no longer corresponds to a plane wave. More comparisons are presented by Scarton (1970).

A further study of the effect of viscosity on the A-band modes shows that it creates behaviour of a boundary-layer type very near the wall, with the vorticity attaining a maximum at the wall and diffusing into the fluid mainstream. Burns (1966, p. 89; 1967) has observed this phenomenon for mode $A0$ for the case of a gas-filled rigid tube undergoing steady-periodic oscillation. A recasting of

Burns's results for mode $A0$† shows that the solution for mode $A0$ can be considered as the sum of two waves. The dominant contribution is a well-behaved wave that does not fluctuate appreciably across the cross-section of the tube. At low frequency and low viscosity, the pressure that gives rise to this wave does not differ greatly from the pressure that is characteristic of propagation in unbounded media. In addition, there is a rotational vorticity wave, generated by viscous shear, that enables the solution to satisfy the boundary condition on the tangential particle velocity at the tube wall. This latter wave appears in the form of a highly damped, oscillatory diffusion wave that is dragged along by the dominant pressure wave. This diffusion wave attains its maximum at the wall, where the interaction of the wall and the oscillating fluid mainstream have created a viscous (or rotational) boundary layer. When $F > F_{LI}$, the diffusion wave is exponentially small in the mainstream. This shear-induced transverse vorticity diffusion wave gives rise to a skin-depth or boundary-layer effect in which steep transverse gradients of viscous shear exist. Burns computes the thickness of this boundary layer, which in dimensionless form is given by

$$\Delta_{A0} = \delta_{A0}/R = (2D/F)^{\frac{1}{2}} = \sqrt{2}/S_{wn} = 2\sqrt{2}/\sqrt{S_n},$$

where S_{wn} is the shear wavenumber and S_n is the Stokes number (steady-periodic Reynolds number). At the critical dimensionless frequency F_{LI}, Δ_{A0} is 0·24. Examination of the vorticity for the higher numbered A-band modes shows a similar skin-depth effect, with the vorticity for the higher number A-band modes penetrating radially farther into the fluid mainstream than the vorticity for the lower numbered A-band modes. This larger skin depth for the higher A-band modes is to be expected, given the earlier observation that these modes are approaching the non-inertial zero-frequency Fitz-Gerald solutions (cf. § 4.2). The axial spatial attenuation of the backward-propagating modes becomes successively more severe.

For low frequency and high viscosity (e.g. for $F = 10^{-2}$ and $D = 10^{-2}$, figure 6*a*), the real and imaginary parts of the axial velocity profiles for mode $A0$ are essentially parabolic, while the radial velocity resembles a half sine wave in its real and imaginary parts, with the respective dimensionless maxima being at least two orders of magnitude smaller than the dimensionless axial velocity, whose real and imaginary parts are of the same order. Turning next to the opposite extreme of large intermediate frequency and low viscosity (e.g. for $F = 10^{-1}$ and $D = 10^{-4}$, figure 7*a*), markedly different behaviour for the mode $A0$ velocity is observed, the axial velocity being constant and pure imaginary except in a very thin boundary layer and the radial velocity varying linearly with radius except in the boundary layer. Again, the maximum magnitude of the dimensionless axial velocity is many orders larger than the magnitude of the maximum dimensionless radial velocity. These two extremes in behaviour for the mode $A0$ velocity are well-known (Schlichting 1960, pp. 229–231), the former representing time-varying quasi-steady Poiseuille flow and the latter Richardson's 'annular effect', the distinction being caused by the depth of

† The ratio of specific heats $\gamma = c_p/c_v$ for a liquid is nearly one; this decouples the nonlinear thermal effect which would otherwise appear.

penetration of the wall shear. (The existence of the thin boundary layer and the resultant extremely steep gradients at the higher frequencies shows that the mode $A0$ axial velocity profiles should indeed be very sensitive to slight numerical errors in the complex $A0$ eigenvalue.)

5.4. *Study of the B-band modal structure*

The vorticity (or rotation) dominance of the B band can be further illustrated by noting that γ_{B0} is directly related to the viscous boundary-layer thickness Δ_{A0} and by observing that the exact analytical solution (21) for γ_{B0} is identical to that obtained for Stokes's second problem, i.e. the flow near an oscillating flat plate (Schlichting 1960, p. 75). Examination of the diffusion equation (4) for $\psi^*_\theta = \mathrm{Re}\{\psi^*_\theta(\mathscr{R})\exp[Z(iF/D)^{\frac{1}{2}} + iFT]\}$ using γ_{B0} gives a reduced ordinary differential equation in $\psi^*_\theta(\mathscr{R})$ where the Z dependence, and thus the diffusion effect, cancels. Apparently, mode $B0$ is excited primarily by an axisymmetric tangential oscillation of the axisymmetric surface mentioned in § 2. This tangential oscillation generates in the fluid rotational shear (or vorticity) waves propagating in the Z direction. Additional proof of the rotational dominance of mode $B0$ comes from observing that its attenuation constant is infinite and its phase velocity zero for zero viscosity. As the vorticity is also zero for zero viscosity, it can be inferred that the B band does not exist for an inviscid fluid. For non-zero viscosity, γ_{B0} is bounded and the vorticity is non-zero, so that shear gradients exist. These same conclusions apply to all B-band modes, as their trajectories all follow the trend set by $B0$.

The radial variation of vorticity for mode $B0$ is found from (24) and (22) using (21) for γ_{B0}, the initial result being indeterminate; use of L'Hospital's rule shows that $\Omega^*_{\theta B0}$ varies linearly with radius $\mathscr{R}$, and is given by

$$\Omega^*_{\theta B0} = \mathrm{Re}\{C^*_{1B0}\mathscr{R}(\gamma_{B0}M_{B0}J_1(M_{B0}))\exp(iFT + \gamma_{B0}Z)\}. \tag{25}$$

For the low-frequency case ($F = 0{\cdot}01$) shown in figure 6, the vorticity for mode $A0$ also has a linear variation, apparently the consequence of the mode degeneracy discussed in § 4.1, where it was shown that γ_{A0} and γ_{B0} approach each other as the frequency tends to zero. The vorticity of the $B1$ mode and higher B-band modes is always complex, its real and imaginary parts being within one order of magnitude of each other.

An examination of the B-band modal pressure shows diffusional behaviour which is identical to that exhibited by the A-band vorticity. In fact, close comparison of the A-band vorticity curves and the B-band pressure curves shows that the former curves can be obtained from the latter curves, to within two-place accuracy, by merely switching real and imaginary parts of the A-band vorticity curves and then changing the signs of the new real and imaginary parts.

Since the roles of pressure and vorticity have apparently been reversed for band A and band B, the conclusions for band A serve to elucidate the physical processes occurring in the $B0$ mode. The dominant contribution to $B0$ is a vorticity wave having a linear radial variation. In addition, there is a pressure wave generated as a consequence of the rigid wall. This latter wave appears in the form of a highly damped, oscillatory diffusion wave that is dragged along

by the dominant vorticity wave. This diffusion wave attains its maximum at the wall, where the interaction of the wall and the oscillating fluid mainstream have created a quasi-boundary layer near the wall. When $F > F_{LI}$ the diffusion wave is exponentially small in the fluid mainstream. The expression 'quasi-boundary layer' is used because the exact mechanism which creates this B-band boundary layer does not appear to be shear, since the vorticity is generally non-zero across the entire cross-section of the tube. It seems likely that the mechanism which creates this quasi-boundary layer is a secondary dilatational interaction between the fluid mainstream and the rigid wall, since the diffusional B-band quantity is pressure. The reason for the existence of this diffusive pressure wave close to the wall is most easily visualized by considering the exciting axisymmetric tangentially oscillating surface to be flat so that the tangential oscillations are radial, i.e. a radially expanding and contracting flat piston. Under this condition the oscillation would produce transverse shear waves whose displacements would be perpendicular to the tube wall. In the region of fluid nearest the tube wall the radially oscillating perpendicular fluid displacements would tend to impact the wall, compressing the fluid adjacent to the wall and thus creating the above-mentioned radial diffusional pressure or dilatation waves. Therefore, a plausible name for this B-band quasi-boundary layer is a *dilatational boundary layer*. As with the A-band vorticity, this pressure diffusion wave gives rise to a skin-depth effect. The penetration depth Δ_{B0} can be defined by simply $\Delta_{A0} = \Delta_{B0}$. Thus, the spatial attenuation and skin depth for mode $B0$ are equal at $(2D/F)^{\frac{1}{2}}$, so, as has been pointed out by Lighthill (1971, private communication), for $F > 2D = F_{LI}/17{\cdot}5$ the dilatational boundary layer reduces to a corner effect. The higher numbered B-band pressure modes show a similar skin-depth effect, with the pressure for the higher numbered B-band modes penetrating farther into the fluid mainstream than the pressure for the lowered numbered B-band modes. As with the A-band modes, this larger skin depth for the B-band modes is to be expected, given the nearness of the non-inertial zero-frequency Fitz-Gerald solutions (cf. § 2). The axial spatial attenuation becomes successively more severe for the higher numbered B-band modes. It should be pointed out that under normal circumstances the tangential oscillation of the disturbing surface would be difficult to produce, so that in the usual case of an axially oscillating flat piston, the principal function of B-band modes would be to help to satisfy the no-slip condition on the piston face, and thus, to help to proportion the input piston radiation of energy properly.

An examination of the mode $B0$ radial and axial velocities in figures 6 and 7 shows that the general appearance is similar to that of the $A0$ velocity profiles. At low frequency and high viscosity (e.g. for $F = 10^{-2}$ and $D = 10^{-2}$, figure 6*a*), an equivalent time-varying 'Poiseuille' flow is observed, while at higher frequency and lower viscosity (e.g. for $F = 10^{-1}$ and $D = 10^{-4}$, figure 7*a*), mode $B0$ is found to describe behaviour equivalent to Richardson's 'annular effect'. The low-frequency case suggests that the presence of fluid compressibility is felt throughout the entire fluid cross-section, while the intermediate-frequency case suggests that the presence of fluid compressibility is felt only in the very thin dilatational boundary layer, with the fluid mainstream acting as if it were incompressible.

There is a major difference between the A-band and B-band modal velocities: whereas the maximum magnitudes of the complex dimensionless A-band radial and axial velocity components are at least two orders apart, the maximum magnitudes of the dimensionless B-band velocity components are of the same order. This difference in behaviour is to be expected, given the above-mentioned tangential excitation of these latter modes.

6. Comments on the general n homogeneous boundary conditions problem

Study of the preceding linear solution with two homogeneous radial boundary conditions, which yield two bands of complex eigenvalues, suggests an extrapolation of the findings to the general problem where n homogeneous boundary conditions must be satisfied as follows. A temporally stable steady-state linear oscillating continuous system constrained by n homogeneous boundary conditions will possess n bands of complex eigenvalues for waves of positive radiation condition and n bands of complex eigenvalues for waves of negative radiation condition. Further, for all waves with radiation conditions of like sign, n end conditions will be required.

An application of this extrapolation to the problem considered by Burns (1967) (i.e. the above viscous solution but with the compressible liquid changed to a gas so that the temperature can become important, and where the waves are initiated by a flat axially oscillating piston which can be at a temperature different from that of the tube wall) is mentioned by Scarton (1970). The procedure for computing the net profiles will be outlined in a later paper, which will contain a more amplified and complete development of the synthesis problem than was given by Scarton (1970).

This work was done in the Department of Mechanical Engineering at Carnegie-Mellon University in partial fulfilment of the requirements for the degree of Doctor of Philosophy by Henry A. Scarton. It was supported jointly by a National Science Foundation Traineeship and Ford Foundation grant to H. A. S., and National Science Foundation Grant GK-2542. The authors are grateful to Professor Sir James Lighthill, Dr H. K. Moffatt, Professor W. F. Hughes, Dr. S. Richardson and Professor H. F. Tiersten for their assistance and helpful comments. The calculations were performed on the Univac 1108 computer of Carnegie-Mellon University. L. Raab and D. Rao assisted in data handling.

Note added in proof. The zero-frequency limit discussed at the end of §4 results in some interesting conclusions regarding the form of ϕ and $\boldsymbol{\psi}$. Sternberg (1960) (and also Gurtin 1972) discusses this limit in the use of Lamé potentials in the Helmholtz decomposition for the solution of the equations of elasticity: the resultant *static equilibrium* displacement field is shown to be the sum of the *time-dependent* scalar and vector potentials, the time dependence of which cancels upon addition.

REFERENCES

BROWN, F. T. 1962 Transient response of fluid lines. *Trans. A.S.M.E., J. Basic Engng*, D **84**, 547–553.

BURNS, S. H. 1966 Finite-amplitude travelling waves with boundary dissipation. *Harvard Univ. Acoust. Res. Lab. Tech. Memo.* no. 60.

BURNS, S. H. 1967 Finite-amplitude distortion in air at high acoustic pressures. *J. Acoust. Soc. Am.* **41**, 1157–1168.

COHEN, H. & TU, Y. 1962 Viscosity and boundary effects in the dynamic behavior of hydraulic systems. *Trans. A.S.M.E., J. Basic Engng*, D **84**, 593–601.

ELCO, R. A. & HUGHES, W. F. 1962 Acoustic waveguide mode interference and damping with viscous fluids. *4th Int. Congr. Acoustics, Copenhagen*, pp. 21–28.

FITZ-GERALD, J. M. 1969 Blood flow in narrow capillaries. Ph.D. dissertation, Imperial College, London.

FITZ-GERALD, J. M. 1972 Plasma motions in narrow capillary flow. *J. Fluid Mech.* **51**, 463–476.

GERLACH, C. R. & PARKER, J. D. 1967 Wave propagation in viscous fluid lines including higher mode effects. *Trans. A.S.M.E., J. Basic Engng*, D **89**, 782–788.

GURTIN, M. E. 1972 The linear theory of elasticity. *Handbuch der Physik* (ed. C. Truesdell), VIa/2, pp. 232–242. Springer.

IBERALL, A. S. 1950 Attenuation of oscillatory pressures in instrument lines. *Nat. Bur. Stds. J. Res.* **45**, 85–108.

KIRCHHOFF, G. 1868 Über den Einfluss der Wärmeleitung in einen Gase auf die Schallbewegung. *Ann. Phys. Chem.* **134**, 177–193.

LIGHTHILL, M. J. 1956 Viscosity effects in sound waves of finite amplitude. In *Surveys in Mechanics* (ed. G. K. Batchelor & R. M. Davies), pp. 251–350. Cambridge University Press.

LIGHTHILL, M. J. 1965 Group velocity. *J. Inst. Maths. Applics.* **1**, 1–28.

NEHARI, Z. 1965 *Introduction to Complex Analysis.* Allyn & Bacon.

OLSON, R. M. 1962 *Engineering Fluid Mechanics.* International Textbook Co.

ONOE, M., MCNIVEN, H. D. & MINDLIN, R. D. 1962 Dispersion of axially symmetric waves in elastic rods. *Trans. A.S.M.E., J. Appl. Mech.* E **84**, 729–734.

RAYLEIGH, LORD 1896 *The Theory of Sound.* Dover.

REDWOOD, M. 1960 *Mechanical Waveguides.* Pergamon.

ROBINSON, E. L. & SCARTON, H. A. 1972 CONTOR: a FORTRAN subroutine to plot smooth contours of a single-valued arbitrary three-dimensional surface. *J. Comp. Phys.* **10**, 242–251.

ROSENHEAD, L. 1954 The second coefficient of viscosity: a brief review of fundamentals. *Proc. Roy. Soc.* A **226**, 1–6.

RUBINOW, S. I. & KELLER, J. B. 1971 Wave propagation in a fluid filled tube. *J. Acoust. Soc. Am.* **50**, 198–223.

SCARTON, H. A. 1970 Waves and stability in viscous and inviscid compressible liquids contained in rigid and elastic tubes by the method of eigenvalleys. Ph.D. dissertation, Carnegie-Mellon University, Pittsburgh. (Available from *University Microfilms*, Ann Arbor, Michigan 48106: order no. 70-18, 029E.)

SCARTON, H. A. 1971 Double precision FORTRAN subroutines to compute both ordinary and modified Bessel functions of the first kind and of integer order with arbitrary complex argument: $J_n(x+jy)$ and $I_n(x+jy)$. *J. Comp. Phys.* **8**, 295–299.

SCARTON, H. A. 1973 The method of eigenvalleys. *J. Comp. Phys.* **11**, 1–143.

SCHLICHTING, H. 1960 *Boundary Layer Theory.* McGraw-Hill.

SERGEEV, S. I. 1966 Fluid oscillations in pipes at moderate Reynolds numbers. In *Fluid Dynamics*, vol. 1, pp. 121–122. Faraday Press.

SHIELDS, F. D., LEE, K. P. & WILEY, W. J. 1965 Numerical solution for sound velocity and absorption in cylindrical tubes. *J. Acoust. Soc. Am.* **37**, 724–729.

STERNBERG, E. 1960 On the integration of the equations of motion in the classical theory of elasticity. *Arch. Rat. Mech. Anal.* **6**, 34–50.

TIJDEMAN, H. 1969 Remarks on the frequency response of pneumatic lines. *Trans. A.S.M.E., J. Basic Engng*, D **91**, 325–327.